Femtosecond Optical Generation and Detection of Coherent Acoustic Phonons in GaN Single Crystals

Introduction

Coherent acoustic phonons (CAP's) excited by ultrafast laser pulses have been investigated using optical pump/probe spectroscopy in GaN systems, including GaN thin films, $In_xGa_{1-x}N$/GaN heterostructures, and multiple quantum wells.[1–5] A common feature of such structures is the existence of a significant lattice mismatch, which results in highly strained interfaces. Since GaN and its alloys are piezoelectric semiconductors with large piezoelectric constants, the presence of strain at the interface gives rise to a strong, of-the-order-of-several-MV/cm,[5] built-in piezoelectric field. When a pump-laser pulse excites electron-hole pairs, the strain-induced piezoelectric field spatially separates the electrons and holes and, in turn, leads to a stress that serves as the source of CAP generation.

In addition to the piezoelectric effect, two other CAP-generation mechanisms have been reported in the literature:[6,7] the deformation-potential–coupled electronic stress and the heat-induced thermal stress. Both of these stresses originate in the transient photoexcitation of electron-hole pairs in the material. In one case, the transition of electrons from the valence band to the conduction band breaks the lattice equilibrium and results in a deformation of the lattice. Such deformation, in turn, alters the semiconductor band structure and induces the electronic stress coupled to the conduction-band free carriers through the deformation potential. In the other case, the photoexcited carriers simply transfer their excess energy to the lattice via electron–phonon scattering, as they relax down toward the band edge. The fast cooling process of hot carriers produces a sharp increase in the lattice temperature, leading to thermal stress.

Among the above-mentioned mechanisms of CAP generation, the piezoelectric effect always makes the dominant contribution in the strained systems, studied in Refs. 1–5, while the other two typically play only a very weak role, as discussed in Ref. 5. However, in bulk semiconductor single crystals (GaN, in our case), there is obviously no lattice-mismatch–induced strain and the piezoelectric field cannot be built. Thus, the CAP generation can only be due to either the electronic or thermal stress, or both, depending on the photon excitation energy and the studied material's properties.

In recent work,[8] we have demonstrated that in bulk GaN crystals the stress-induced CAP's are very long lived and propagate macroscopic distances without losing their coherence. We utilized far-above-bandgap, ultraviolet (UV) femtosecond pump pulses to excite the CAP's at the sample surface and detected them by measuring the transient differential reflectivity ($\Delta R/R$) signal of a time-delayed, near-infrared (NIR) probe pulse. We observed the CAP oscillations (superimposed on the exponentially decaying $\Delta R/R$ electronic transient) with the amplitude of the order of 10^{-5} to 10^{-6} and the frequency linearly dependent (no dispersion) on the probe-beam wave number. We have also made an early prediction that the electronic stress was the dominant factor in CAP generation in bulk GaN crystals.

In this work, we report our systematic experimental and detailed theoretical modeling studies on all-optical generation and detection of CAP's in bulk GaN crystals with the two-color (UV/blue–NIR), time-resolved, femtosecond pump/probe technique. Our theoretical modeling is based on the one-dimensional elastic wave equation and diffusion effects and predicts that the electronic stress is the dominant factor in CAP generation in GaN single crystals. For a CAP-detection mechanism, we have derived an analytic expression for the time-dependent, probe-beam reflectivity change caused by the propagating CAP's. Experimentally, we have varied the energy of the pump excitation pulses from far above the GaN bandgap, through near bandgap, up to just below bandgap (band-tail states). In all cases, we were able to produce easily measurable CAP oscillations, and, by careful investigation of their amplitude changes as a function of the energy (wavelength) of the pump photons, we confirmed that indeed the CAP excitation origin was due to the electronic stress, generated by the femtosecond pump at the sample surface region. By using, in all of our tests, probe beams with photon energies far below

the GaN bandgap (corresponding wavelengths were around 800 nm), we took advantage of a very small, ~50-cm^{-1} absorption coefficient (very weak attenuation) of probe light in GaN crystals[8,9] and were able to demonstrate that the CAP pulses propagated deeply into the GaN crystal volume without any measurable loss of coherence/attenuation.

Another advantage of our two-color pump/probe configuration was that the NIR probe was not sensitive to the details of the band-gap structure, nor to any interband absorption.[10] The possibility of the two-photon–absorption process was also negligible because the total energy of two ~800-nm probe photons was still considerably lower than the GaN bandgap energy. Thus, the UV–NIR, two-color femtosecond spectroscopy allowed us to avoid any undesired effects and made our phonon dynamics studies in GaN very clear to interpret.

In the next section we present our theoretical approach to the phenomenon of acoustic phonon generation and their coherent propagation in bulk semiconducting single crystals, stressing the need to include both electronic and thermal stresses in the phonon-generation mechanism. We also demonstrate that under our experimental conditions, for GaN, the amplitude of the CAP's depends only on the energy/wavelength of pump photons, while their oscillation frequency is probe dependent only in the simplest-possible dispersionless manner. The last two sections (1) briefly review our GaN crystal growth, describe the two-color femtosecond spectroscopy setup used in our measurements, and present detailed experimental results and their interpretation; and (2) present our conclusions and underline the applicability of our theoretical model for CAP studies in any high-quality single-crystal semiconducting materials.

Theoretical Modeling

Following the approach presented by Thomsen *et al.*,[7] we have developed a theoretical model of the generation, propagation, and detection of CAP's in bulk GaN crystals, studied using a femtosecond, two-color pump/probe technique. In our scheme, an intense, femtosecond laser pump pulse with photon energy above the material bandgap excites both the electronic and thermal stresses at the sample surface. These two stresses act as the driving terms in the elastic wave equation that describes generation and propagation of CAP's. The propagating CAP's modulate optical properties of the GaN dielectric function, which is represented as disturbance of a dielectric permittivity in Maxwell's equations. By solving the Maxwell equations, we obtained an analytical expression for the time-dependent modulation of the $\Delta R/R$ transient caused by the traveling CAP waves, which, in turn, could be directly measured in our experiments, using below-bandgap probe pulses.

We stress that the Thomsen model was developed to explain generation and detection of CAP's in $\alpha - As_2Te_3$ and similar compounds with a picosecond, one-color pump/probe method.[7] In such a case, the CAP generation was assumed to be solely due to the thermal stress, and the detection was limited in a near-surface region. In the model presented here, we will consider both the electronic- and thermal-stress generation mechanisms. Since GaN exhibits relatively large deformation potential and different coefficients in ambipolar and thermal diffusion, the contribution of the electronic stress to the CAP's amplitude and shape is different from that of the thermal stress. Our theoretical calculations show that in GaN, CAP's generated by electronic stress have actually an-order-of-magnitude-larger strength than that generated by the thermal stress.

In the experimental CAP detection, we use far-below-bandgap femtosecond probe-beam pulses. For bulk samples, surface-generated CAP's propagate forward into the material with no reflections toward the surface. Thus, the surface (one-color scheme) detection scheme that was used by Thomsen *et al.*[7] to detect the echo of a CAP pulse is not appropriate in our case. In contrast, by using a far-below-bandgap probe beam, we were able to detect the CAP perturbation propagating deeply inside the material, taking advantage of the very long penetration depth (very low absorption) of our NIR probe photons.

1. CAP Pulse Generation

We consider a femtosecond UV pump pulse with photon energy higher than the GaN bandgap that is incident on the surface of a bulk GaN crystal. Given that the diameter of the irradiated area is much larger than the UV pulse absorption depth, both the electronic and thermal stresses generated by the pump pulse can be assumed to depend only on the z axis, which is defined to be perpendicular to the sample surface and pointing into the sample. Therefore, the lattice displacement has a nonzero component only in the z direction, and, in our case, the CAP generation is reduced to a one-dimensional (1-D) problem.

The 1-D elastic (nondissipative) wave equation describing generation and propagation of CAP's is given by

$$\frac{\partial^2 \eta_{zz}(z,t)}{\partial t^2} - v_s^2 \frac{\partial^2 \eta_{zz}(z,t)}{\partial z^2} = \frac{1}{\rho}\frac{\partial}{\partial z^2}\left(\sigma_{zz}^{\text{th}} + \sigma_{zz}^{e}\right), \qquad (1)$$

where $\eta_{zz}(z,t) = \partial u(z,t)/\partial z$ represents the acoustic phonon field with $u(z,t)$ defined as the lattice displacement, v_s is the longitudinal sound velocity in GaN, ρ is the mass density of GaN, and σ_{zz}^{th} and σ_{zz}^{e} are the thermal and electronic stresses, respectively. Both σ_{zz}^{th} and σ_{zz}^{e} are functions of z and time t and can be expressed as

$$\sigma_{zz}^{\text{th}}(z,t) = -3B\beta\Delta T(z,t), \tag{2}$$

$$\sigma_{zz}^{e}(z,t) = d_c n_e(z,t) - d_v n_h(z,t), \tag{3}$$

where B is the bulk modulus, β is the linear thermal expansion coefficient, $\Delta T(z,t)$ is the lattice temperature rise, d_c and d_v are the conduction-electron and valence-hole deformation potentials, respectively, and, finally, $n_e(z,t)$ and $n_h(z,t)$ are the photoexcited electron and hole densities, respectively. In general, $n_e(z,t)$ and $n_h(z,t)$ have different spatiotemporal evolutions, but, since in our case they are initially excited in equal numbers by the same pump pulse, we are going to ignore this difference and assume that $n_e(z,t) \approx n_h(z,t) = n(z,t)$, and, hence, Eq. (3) becomes

$$\sigma_{zz}^{e}(z,t) = (d_c - d_v)n(z,t). \tag{4}$$

Assuming that both the carrier motion and heat conduction have a diffusive character, we utilize a simple transport model to describe the evolution of $n(z,t)$ and $\Delta T(z,t)$:

$$\frac{\partial n(z,t)}{\partial t} - D\frac{\partial^2 n(z,t)}{\partial z^2} = 0, \tag{5}$$

$$\frac{\partial \Delta T(z,t)}{\partial t} - \chi\frac{\partial^2 \Delta T(z,t)}{\partial z^2} = 0, \tag{6}$$

with the initial conditions

$$n(z,0) = \frac{\alpha_{\text{pump}}(1-R_{\text{pump}})Q}{E_{\text{pump}}}\exp(-\alpha_{\text{pump}}z), \tag{7}$$

$$\Delta T(z,0) = \frac{\alpha_{\text{pump}}(1-R_{\text{pump}})Q}{E_{\text{pump}}} \times \frac{E_{\text{pump}} - E_g}{C_V}\exp(-\alpha_{\text{pump}}z), \tag{8}$$

and boundary conditions

$$D\frac{\partial n(0,t)}{\partial z} = 0, \tag{9}$$

$$\chi\frac{\partial \Delta T(0,t)}{\partial z} = 0, \tag{10}$$

where D is the ambipolar diffusion coefficient of the GaN electron-hole plasma; χ is the thermal diffusivity; R_{pump}, Q, α_{pump}, and E_{pump} are the reflectance, fluence, absorption coefficient, and photon energy of the pump beam; and E_g and C_V are the GaN bandgap energy and the specific heat per unit volume, respectively. We have also assumed above that during the duration of our ~150-fs-wide pump pulses, the photoexcitation is instantaneous and the plasma diffusion is negligible.

Knowing the $n(z,t)$ and $\Delta T(z,t)$ distributions, we can readily solve the wave equation [Eq. (1)], subject to the initial, $t = 0$, and elastic boundary, $z = 0$, conditions:

$$\eta_{zz}(z,0) = 0, \tag{11}$$

$$\eta_{zz}(0,t) = \frac{1}{\rho V_s^2}\left[3B\beta\Delta T(0,t) - (d_c - d_v)n(0,t)\right]. \tag{12}$$

In our analysis of CAP generation, the two trigger mechanisms, namely, the electronic and thermal stresses, are completely decoupled. Thus, the CAP fields excited by each mechanism can be treated separately, and the total CAP field is just the simple sum of both the electronic and thermal components. Figure 110.27 presents examples of numerically computed profiles of CAP transients, generated by the electronic stress, the thermal stress, and the sum of both, respectively. The CAP pulses plotted in Fig. 110.27(a) were calculated for the far-above-bandgap pump-photon excitation (photon energy of 4.59 eV; corresponding wavelength 270 nm), while those shown in Fig. 110.27(b) correspond to the excitation using just-above-bandgap pump photons (energy of 3.54 eV; wavelength 350 nm). In both cases, Q was kept constant and equal to 0.08 mJ/cm^2/pulse, the value actually implemented in our pump/probe experiments, while the α_{pump} values were taken to be 2.07×10^5 and 1.29×10^5 cm^{-1}, corresponding to the pump-photon energies of 4.59 eV and 3.54 eV, respectively.[9] The other GaN material parameters used in our calculations can be found in Table 110.III.

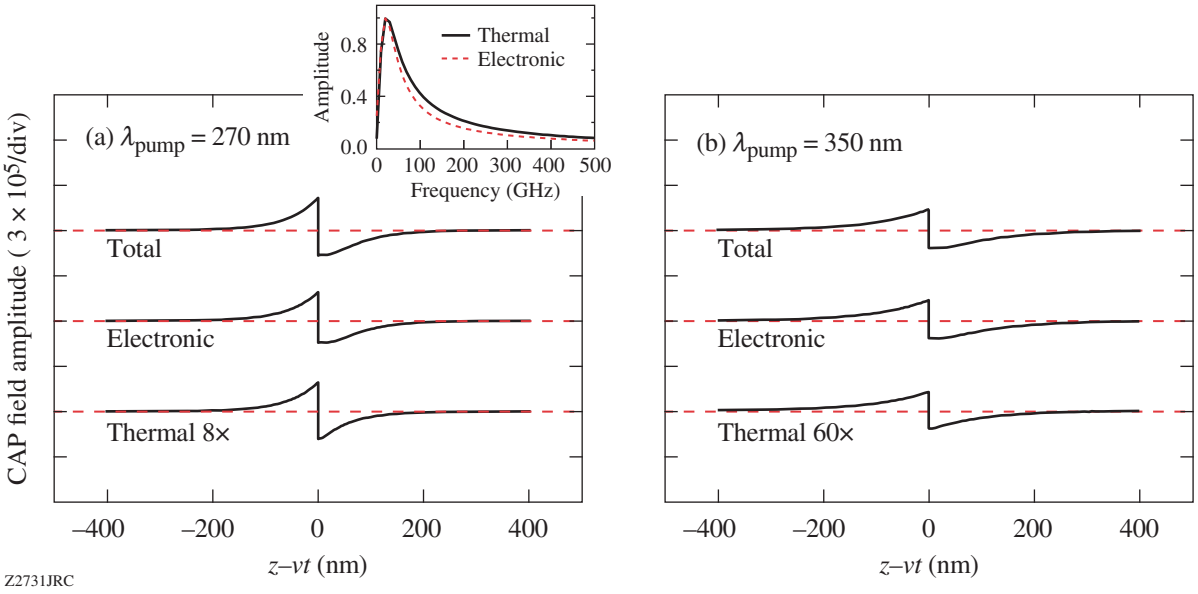

Figure 110.27
Simulation of spatial-time profiles of propagating CAP transients generated by the electronic stress, thermal stress, and the sum of both, respectively. The CAP pulses shown in (a) and (b) were excited by the pump photons with photon energies of 4.59 eV and 3.54 eV (wavelengths 270 nm and 350 nm), respectively. The inset shows the frequency spectra of the electronically (solid line) and thermally induced (dashed line) CAP.

Table 110.III. Material parameters for wurtzite GaN.

Parameter	GaN
Longitudinal sound velocity v_s (m/s)	8020[11]
Mass density ρ (g/cm^3)	6.15[12]
Bulk modulus B (GPa)	207[13]
Linear thermal expansion coefficient β (K^{-1})	3.17×10^{-6}[14]
Electron deformation potential d_c (eV)	–4.08[15]
Hole deformation potential d_v = D1 + D3 (eV)	2.1[16]
Ambipolar diffusion coefficient D (cm^2/s)	2.1[17]
Thermal diffusivity χ (cm^2 s^{-1})	0.43[12]
Band gap E_g (eV)	3.4[18]
Specific heat per unit volume C_v (J cm^{-3}°C^{-1})	3.01[12]

As seen in Fig. 110.27, CAP pulses have a strength of the order of 10^{-5} and a spatial width of approximately twice the pump-beam penetration depth $\left(\xi_{pump} = 1/\alpha_{pump}\right)$. We note, however, that our simulations predict that the electronic stress contribution is the major, dominant contribution in CAP generation, as compared to the thermal-stress contribution, in both the far-above- and just-above-bandgap excitations [Figs. 110.27(a) and 110.27(b), respectively], with the strength ratio between the electronic- and thermal-induced CAP's equal to about 8 and 60 for the 4.59- and 3.54-eV pump photons, respectively. The electronically induced strength of CAP's decreases only slightly when the pump photon energy decreases from 4.59 eV to 3.54 eV, while the thermal one drops by about an order of magnitude. Thus, the change of the total CAP strength is small [see Figs. 110.27(a) and 110.27(b), bottom curves], as it is electronically dominated. The CAP amplitude is determined mainly by α_{pump}, which changes only a little in the studied above-bandgap, pump-energy region.

The shapes of all CAP pulses presented in Fig. 110.27 are asymmetrically bipolar with a slight broadening at their trailing sides. This broadening is caused by the diffusion effects[7] and is much more pronounced in the electronically induced CAP's because the electron-hole diffusion is about five times faster than the thermal diffusion. The diffusion effects not only broaden the CAP pulse, but they also narrow its frequency

spectrum [inset in Fig.110.27(a)], where the spectra of the electronically and thermally induced CAP's are shown.

2. CAP Pulse Detection

In the discussed GaN sample geometry, the surface-generated CAP pulses propagate into the crystal along the z axis, causing a spatiotemporal modulation of the material's dielectric function. This modulation can be detected through the change in the reflectivity R of a time-delayed probe beam. The R dependence in the presence of a generalized disturbance of the dielectric function can be obtained by solving the Maxwell equations inside the GaN sample and was derived by Thomsen *et al.*[7] as

$$R = \left| r_0 + \Delta r \right|^2, \tag{13}$$

where

$$r_0 = \frac{1 - n - i\kappa}{1 + n + i\kappa} \tag{14}$$

is the reflection coefficient at the sample surface and represents that part of the probe beam's electric field reflected from the free surface, while

$$\Delta r = \frac{2i\omega}{c(1 + n + i\kappa)^2}\int_0^\infty \mathrm{d}z' e^{2i(n+i\kappa)k_0 z'}\,\Delta\varepsilon(z,t) \tag{15}$$

corresponds to the probe beam's electric field reflected from the CAP pulse. In Eqs. (14) and (15), n and κ are the real and imaginary parts of the refractive index, respectively; ω, c, and k_0 are the angular frequency of the probe light, the light speed, and the wave vector of the probe beam in vacuum, respectively; and $\Delta\varepsilon(z,t)$ is the change in dielectric function, which, under assumption that the disturbance is caused only by the propagating CAP pulse, can be expressed as

$$\Delta\varepsilon(z,t) = 2(n + i\kappa)\left(\frac{\mathrm{d}n}{\mathrm{d}\eta_{zz}} + i\frac{\mathrm{d}\kappa}{\mathrm{d}\eta_{zz}}\right)\eta_{zz}(z,t). \tag{16}$$

Finally, we note that κ is related to the probe-beam absorption coefficient α_{probe} or, equivalently, the penetration depth ζ_{probe} through $\kappa = \alpha_{\text{probe}}\lambda/4\pi = \lambda/4\pi\zeta_{\text{probe}}$, where λ is the probe-beam wavelength.

Since our experiments measure the probe's $\Delta R/R$ signal, Eq. (13) must be rewritten in the form

$$\Delta R/R = \frac{\left| r_0 + \Delta r \right|^2 - \left| r_0 \right|^2}{\left| r_0 \right|^2}. \tag{17}$$

The analytic expression of $\Delta R/R$ can be obtained if $n_{zz}(z,t)$, which we have only in a numerical form presented in Fig. 110.27, is substituted in Eq. (16) by an analytic expression:

$$\eta_{zz}(z,t) = -Ae^{-\alpha_{\text{pump}}\left| z - v_s t \right|}\operatorname{sgn}\left(z - v_s t\right), \tag{18}$$

which fits our stress pulses very well and neglects only the electron-hole and thermal diffusion effects in the CAP generation, and A is the strength of the CAP pulse given by

$$A = \frac{\alpha_{\text{pump}}\left(1 - R_{\text{pump}}\right)Q}{2E_{\text{pump}}\rho v_s^2} \times \left[-\left(d_c + d_v\right) + \frac{3B\beta}{C_V}\left(E_{\text{pump}} - E_g\right)\right]. \tag{19}$$

Combining the above formulas and considering that for our two-color pump/probe technique the condition $\alpha_{\text{pump}} \gg \alpha_{\text{probe}}$ holds, we find an analytic expression for $\Delta\varepsilon(z,t)$ and, finally, obtain the closed-form formula for $\Delta R/R$, correct to the first order in $n_{zz}(z,t)$:

$$\Delta R/R = \sqrt{\left(\frac{\mathrm{d}n}{\mathrm{d}\eta_{zz}}\right)^2 + \left(\frac{\mathrm{d}\kappa}{\mathrm{d}\eta_{zz}}\right)^2}\,AF_1 \times \left[\sin\left(\frac{4\pi n v_s t}{\lambda} - \phi\right)e^{-v_s t/\zeta_{\text{probe}}} + F_2 e^{-v_s t/\zeta_{\text{pump}}}\right], \tag{20}$$

where

$$F_1 = \frac{\sqrt{n^2\left(n^2 + \kappa^2 - 1\right)^2 + \kappa^2\left(n^2 + \kappa^2 + 1\right)^2}}{n\left(n^2 + \kappa^2 + 1\right)^2 - 4n^3} \tag{21}$$

is the probe-beam–related amplitude,

$$\phi = \arctan\left[\frac{\kappa\left(n^2 + \kappa^2 + 1\right)}{n\left(n^2 + \kappa^2 - 1\right)}\right]\arctan\left[\frac{\mathrm{d}n/\mathrm{d}\eta_{zz}}{\mathrm{d}\kappa/\mathrm{d}\eta_{zz}}\right] \tag{22}$$

is the phase, and

$$F_2 = \frac{8\pi^2 n^2 \sin\phi - 2\pi n\lambda\alpha_{\text{pump}}\cos\phi}{16\pi^2 n^2 + \lambda^2\alpha_{\text{pump}}^2}. \quad (23)$$

Equation (20) allows us to directly compare our theoretical modeling with the experiments, facilitating data analysis and making our results more explicit. We can, however, simplify Eq. (20) somewhat further by noting that under our experimental conditions, ζ_{pump} is of the order of several tens of nanometers; thus, for the GaN sound speed v_s = 8020 m/s, the second term in the square bracket in Eq. (20) rapidly damps out within several picoseconds and can be neglected, as in our experiments we study CAP's within at least a few-hundred-ps-wide time delay window. The simplified expression of $\Delta R/R$ can be written as

$$\Delta R/R = \sqrt{\left(\frac{dn}{d\eta_{zz}}\right)^2 + \left(\frac{d\kappa}{d\eta_{zz}}\right)^2} \times AF_1 \sin\left(\frac{4\pi n v_s t}{\lambda} - \phi\right) e^{-v_s t/\zeta_{\text{probe}}}. \quad (24)$$

The temporal dependence of $\Delta R/R$ is represented in Eq. (24) as a simple damped-sinusoidal function and it follows Eq. (48) in Ref. 7, but now we also have an expression for the $\Delta R/R$ amplitude, as the product of A, F_1, and $\sqrt{\left(dn/d\eta_{zz}\right)^2 + \left(d\kappa/d\eta_{zz}\right)^2}$. The probe-related F_1 [see Eq. (21)] can be considered as a constant since for far-below-bandgap NIR light, n and κ in high-quality GaN crystals remain almost unchanged. The $dn/d\eta_{zz}$ and $d\kappa/d\eta_{zz}$ terms are the photoelastic constants and are related only to n and κ; thus, $\sqrt{\left(dn/d\eta_{zz}\right)^2 + \left(d\kappa/d\eta_{zz}\right)^2}$ also contributes a constant term in the total $\Delta R/R$ amplitude. Finally, following Eq. (19), the term A (strength of the CAP pulse) is only pump light related. We note that A experiences a dramatic change when the pump energy is tuned across the band edge because of the step-like change of α_{pump} near E_g. Experimentally it means that the total $\Delta R/R$ amplitude measured using the two-color pump/probe technique should change with the pump-beam energy, following the same functional dependence as A, namely the spectral characteristics of α_{pump}. Furthermore, this theoretical prediction indicates that we should be able to undeniably determine which stress contribution—electronic or thermal—is the dominant factor for triggering the CAP's in our bulk GaN crystals. If the electronic stress is dominant, as we saw in **CAP Pulse Generation** (p. 89), the experimentally observed $\Delta R/R$ amplitude should exhibit only a slight decrease when the pump energy changes from far above to just above bandgap. On the other hand, when the thermal stress is dominant, the oscillation amplitude should experience an-order-of-magnitude drop in the same pump-energy range. Independently, when the pump beam energy is tuned across band edge, the amplitude of the experimental $\Delta R/R$ signal should almost abruptly decrease to zero, due to the rapid decrease of α_{pump}.

In agreement with the Thomsen model,[7] the $\Delta R/R$ damping constant in Eq. (21) is determined by the ζ_{probe}/v_s ratio. For the ~800-nm-wavelength (energy far below the GaN bandgap) probe light used in our two-color measurements, ζ_{probe} is ~200 μm,[8,9] which gives a damping time of ~25 ns. Thus, we should observe CAP's propagating deeply into the GaN crystal, actually, in full agreement with our early studies.[8]

Following again Eq. (24), the frequency of the $\Delta R/R$ oscillations is given by

$$f = 2nv_s/\lambda = \frac{nv_s}{\pi}k_0 \quad (25)$$

and is related only to the probe beam. For a constant n, expected under our experimental conditions, f is proportional to k_0, which indicates a linear dispersion relation for CAP's with the slope corresponding to the fixed v_s. Finally, ϕ [see Eq. (22)] is, in our case, predicted to be a constant.

Experimental Procedures and Results

1. Sample Fabrication and Experimental Setup

Our GaN single crystals were grown with a high-pressure, solution-growth (HPSG) method.[19] The growth process was carried out at an external nitrogen gas pressure of 8 to 14 kbar and temperatures of 1350°C to 1600°C because of the high solubility of GaN in Ga at high temperatures. Nitrogen was first compressed to a 10- to 15-kbar level with a two-step pressure compressor and intensifier and then transported into the metallic Ga melt with a temperature gradient of 5°C to 50°C cm^{-1}. GaN single crystals formed at the cooler zone of the HPSG chamber. They grew up to 1-mm-thick platelets with typical sizes of up to 3 × 4 mm^2. These crystals exhibited an excellent wurtzite crystalline structure according to x-ray diffraction measurements, while their morphology depended on the growth process pressure, temperature range, and nitrogen supersaturation. In our experiments, we have studied a 2.5 × 2.5-mm^2, transparent (slightly brownish) GaN crystal piece that was ~0.4 mm thick.

Two-color, femtosecond pump/probe spectroscopy experiments were performed in a reflection mode using a commercial mode-locked Ti:sapphire laser with a pulse duration

of ~100 fs and repetition rate of 76 MHz. Our experimental setup is schematically shown in Fig. 110.28. In our study, two arrangements were used to generate the pump beam with desired photon energy. One optical path (see Fig. 110.28) was designed to deliver photons with energies in the range of 3.1 to 3.54 eV (wavelength of 400 to 350 nm) in the vicinity of a GaN bandgap of 3.4 eV and was based on frequency doubling of the fundamental Ti:sapphire pulse train. The other included our homemade third-harmonic generator and allowed us to generate pump photons with energies ranging from 4.13 eV to 4.64 eV (wavelength of 300 to 267 nm), far above the GaN bandgap. The pump beam was focused onto the surface of the GaN crystal with a spot diameter of ~20 μm at an incident angle of ~30°. The incident fluence was ~0.08 mJ/cm^2 per pulse and was kept constant while varying the pump-photon energy. Probe pulses were directly generated by the Ti:sapphire laser and had photon energies varying from 1.38 eV to 1.77 eV (wavelengths from 900 nm to 700 nm) far below the GaN gap; their fluence was always much lower (at least by a factor of 10) than that of the pump. The probe beam was delayed with respect to the pump and near-normally incident on the same area on the sample surface with a spot diameter of ~10 μm, and its reflection from the sample surface was filtered from any scattered pump photons and collected by a photodetector connected to a lock-in amplifier. The lock-in amplifier was synchronized with a mechanical chopper that modulated the pump beam at a frequency of ~2 KHz. The lock-in output was sent to a computer for data processing. The magnitude of $\Delta R/R$ that we measured was in the range of 10^{-3} to 10^{-6}.

2. Experimental Results

Typical time-resolved $\Delta R/R$ probe signals from our GaN crystal excited with far-above-bandgap (wavelength of 283 nm) and just-above-bandgap (wavelength of 350 nm) pump photons are shown in Figs. 110.29(a) and 110.29(b), respectively. The corresponding probe wavelengths are 850 nm in Fig. 110.29(a) and 720 nm in Fig. 110.29(b). As we can see, although the two presented $\Delta R/R$ waveforms exhibit different electronic relaxation features, observed during the initial few picoseconds of relaxation and associated with the conduction band inter- and intra-valley electron scattering,[10] both are characterized by the same, few-hundred-ps-long exponential decay, associated

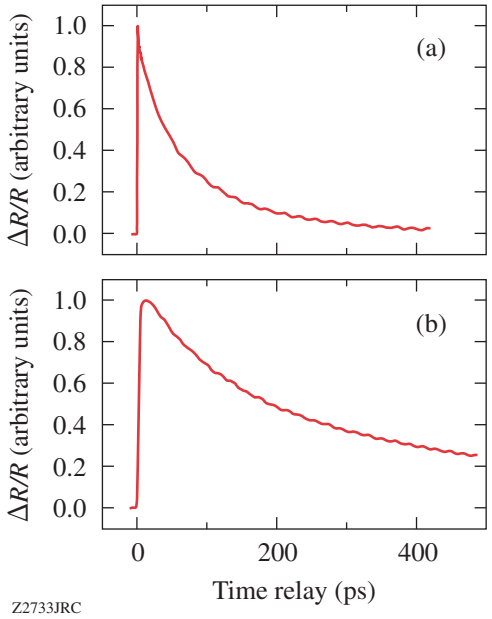

Figure 110.29
Time-resolved normalized $\Delta R/R$ waveforms as a function of the pump/probe delay time, measured in GaN single crystals for (a) the pump/probe wavelength of 283 nm/850 nm; (b) pump/probe wavelength of 360 nm/720 nm. The case (a) corresponds to the far-above-bandgap optical excitation, while case (b) corresponds to just-above-bandgap excitation.

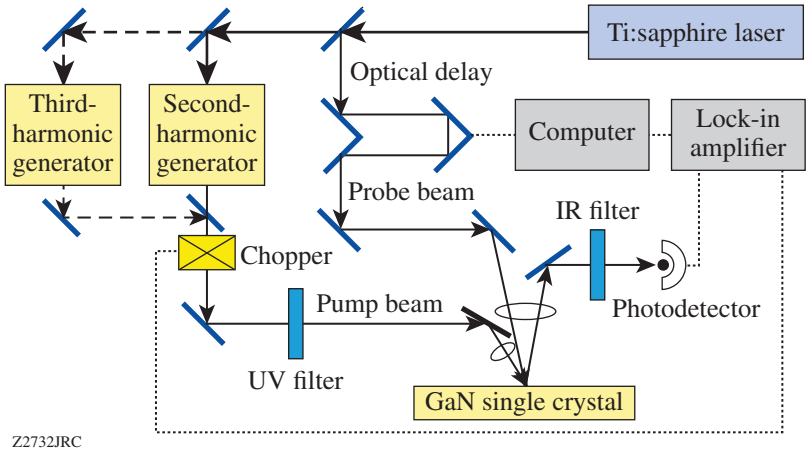

Figure 110.28
Experimental setup for the two-color, femtosecond pump/probe spectroscopy.

with the electron-hole recombination, with pronounced regular oscillations on top of it.

In this work, we focus only on this latter oscillatory feature, which we identify as propagation of the CAP transient inside the crystal.[8] Thus, in order to get a clearer view, we have subtracted numerically the electronic relaxation background from all of our collected raw data. Figure 110.30(a) shows the oscillatory component of the measured $\Delta R/R$ signal for four experimental examples, representative of our measurement cases. The presented traces correspond to the three different experimental conditions for CAP excitation, namely, far-above-bandgap excitation (trace 283 nm/850 nm), just-above-bandgap excitation (traces 350 nm/700 nm and 360 nm/720 nm), and band-tail-state excitation (trace 370 nm/740 nm), respectively. In all cases, no attenuation of the oscillations is observed within our experimental ~450-ps-wide time-delay window, which is consistent with Eq. (24), predicting that in our experiments the CAP oscillation damping constant is limited by the ζ_{probe}/v_s ratio and for $\zeta_{\text{probe}}/v_s \approx 25$ ns is much longer than our experimental time window.

Figure 110.30(b) presents four $\Delta R/R$ CAP-related transients calculated using Eq. (24) and corresponding directly to the four experimental transients shown in Fig. 110.30(a). In our theoretical calculations, the refractive index $n = 2.3$ and the probe absorption coefficient $\alpha_{\text{probe}} = 50\ \text{cm}^{-1}$ are assumed to remain unchanged for all of the studied probe wavelengths. The pump reflectance R_{pump} was set to be 0.2 and the constants $dn/d\eta_{zz}$ and $d\kappa/d\eta_{zz}$ entering into Eqs. (21) and (22) were set to be 1.2 and 0.5, respectively, in order to keep the CAP amplitude term F_1 and phase ϕ consistent with our experimental values. We note that there is extremely good agreement between the corresponding experimental [Fig. 110.30(a)] and theoretical [Fig. 110.30(b)] traces, in terms of both the oscillation amplitude and frequency.

Comparing the traces 283 nm/850 nm, 350 nm/700 nm, and 360 nm/720 nm, we observe only a slight amplitude decrease as we move from the far-above- to just-above-bandgap excitation. On the other hand, the 370-nm/740-nm trace, collected for the pump-photon energy corresponding to GaN band-tail states, has a much smaller amplitude than the other three, but the oscillatory feature is still observable. The above observations experimentally confirm our theoretical prediction that the driving mechanism for CAP generation in bulk GaN crystals is the electronic stress associated with the deformation potential. The rapid drop in CAP amplitude that occurs when we move the energy of our excitation photons across the GaN bandgap (compare traces 360 nm/720 nm and 370 nm/740 nm in Fig. 110.30) is caused by the dramatic change of the α_{pump} coefficient at the band edge. The latter is clearly illustrated in Fig. 110.31, where we plot the experimental CAP oscillation amplitude dependence on the pump-photon wavelength (energy) for the whole pump tuning range. The solid line shows the theoretical $\Delta R/R$ amplitude dependence on the pump-photon energy, using Eq. (24) [see also Eq. (19)]. We used the values listed in Ref. 9 for the α_{pump} spectral dependence in GaN crystals. The solid squares, circles, and triangles represent our experimental data corresponding to the far-above-bandgap, just-above-bandgap,

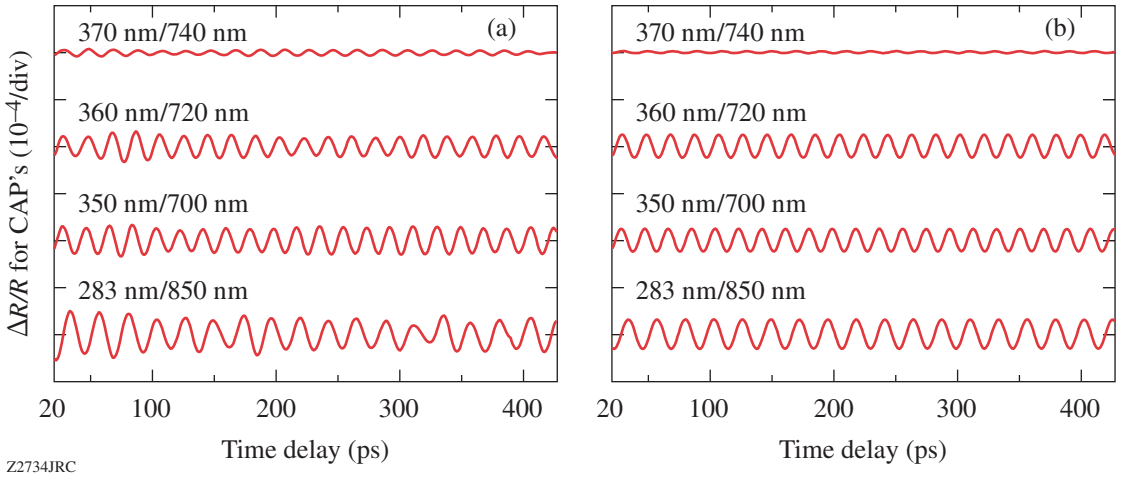

Figure 110.30
The oscillatory components of the $\Delta R/R$ signals as a function of the pump/probe delay time for several pump/probe wavelength configurations: 370 nm/740 nm, 360 nm/720 nm, 350 nm/700 nm, and 283 nm/850 nm. Panels (a) and (b) show the experimental and theoretical results, respectively.

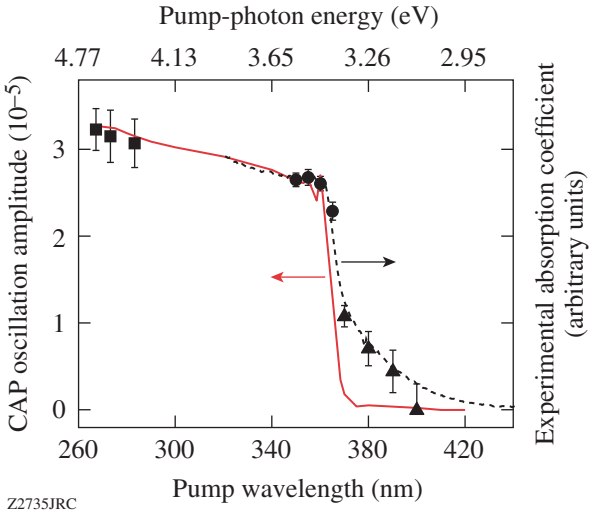

Figure 110.31
The amplitude of the CAP oscillations versus the pump-beam wavelength (energy–top axis). The solid line is the theoretical curve, while the solid squares, circles, and triangles are our experimental data points corresponding to the far-above-bandgap, just-above-bandgap, and band-tail-state pump excitations, respectively. The dashed line (right axis) is the experimental GaN absorption coefficient spectrum, extracted from the transmission and reflection data obtained for our actual GaN single crystal.

and band-tail-state pump excitations, respectively. We see very good overall agreement between our experimental points and the modeling. Only in the case of the pump photons exciting the band-tail states (solid triangles in Fig. 110.31), the decrease of the CAP amplitudes with the pump-wavelength increase is slower than the theoretical prediction. The latter discrepancy, however, is clearly a consequence that in our theoretical calculations we used the values of α_{pump} from Ref. 9 and not α_{pump} directly measured for our GaN samples. The dashed line in Fig. 110.31 corresponds to the GaN absorption coefficient spectrum extracted from the transmission and reflection data of our actual GaN single crystal, experimentally measured using a Perkin-Elmer Lambda 900 spectrophotometer. We note that in this case the agreement is excellent.

For all of the traces plotted in Fig. 110.30, the CAP oscillation phase was essentially constant and equal to ~1.2, as shown in Fig. 110.32, which presents ϕ as a function of the probe-photon wavelength (energy) for our entire experimental tuning range. The constant ϕ is very consistent with our theoretical prediction based on Eq. (22) and the fact that n, κ, $dn/d\eta_{zz}$, and $d\kappa/d\eta_{zz}$ can be assumed constant for our NIR probe photons. The solid line in Fig. 110.32 was obtained by fitting Eq. (20) with $\left(dn/d\eta_{zz}\right)/\left(d\kappa/d\eta_{zz}\right) = 2.5$ as the best fit.

Finally, Fig. 110.33 demonstrates the dispersion relation of the CAP oscillation frequency on the probe beam's wave number. For the entire probe-beam tuning range from 700 nm to 850 nm, we observe a linear (dispersionless) relationship between f and k_0, as predicted by Eq. (25). The slope of the data (solid line in Fig. 110.33) gives v_s = 8002±22 m/s. The

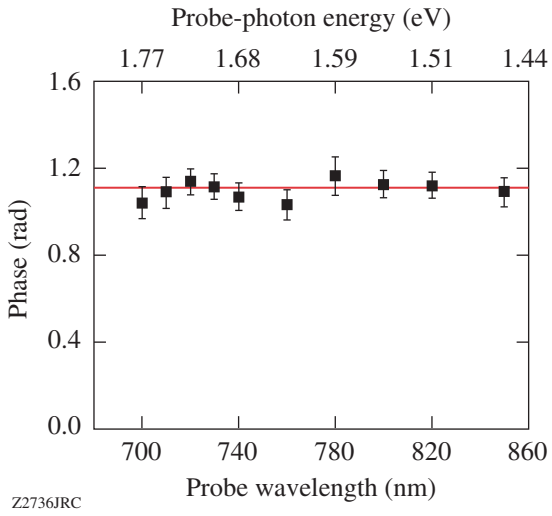

Figure 110.32
The phase of the CAP oscillation versus the probe–beam wavelength (energy–top axis). The solid line shows the theoretical fit based on Eq. (22) with $\left(dn/d\eta_{zz}\right)/\left(d\kappa/d\eta_{zz}\right) = 2.5$.

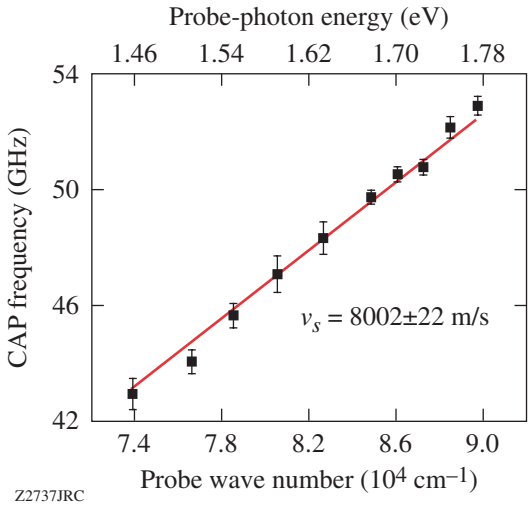

Figure 110.33
The CAP oscillation frequency dependence on the probe beam's wave number (energy–top axis). The solid squares are the peak values of the CAP oscillations Fourier spectra, while the solid line shows the linear fit, intercepting the plot origin, based on Eq. (25).

latter result is very close to our earlier finding,[8] as well as to the values of 8160 m/s and 8020 m/s reported in literature.[1,11]

Conclusions

We have presented our comprehensive studies of CAP generation and detection in a bulk GaN single crystal, using a time-resolved, femtosecond, two-color pump/probe technique. We theoretically predicted and experimentally confirmed that the CAP transients, in our case, were initiated by electronic stress induced at the GaN crystal surface by generation of free carriers, photoexcited by ~100-fs pump UV pulses. Using far-below-bandgap, ~100-fs-wide probe pulses with a very long penetration depth into the GaN crystal, we monitored the CAP propagation that manifested itself as regular, single-frequency oscillations superimposed on the probe $\Delta R/R$ signal. The amplitude of the oscillations was of the order of 10^{-5} to 10^{-6}, and within our ~450-ps time window, we observed no signal attenuation. We also found that the CAP oscillation amplitude was dependent only on the pump-photon energy and, in general, followed the spectral dependence of the GaN optical absorption coefficient, as was predicted by our theoretical model. For the entire tuning range of our NIR probe photons, the phase of the CAP oscillations was constant and the CAP frequency was dispersionless (proportional to the probe k_0) with the slope corresponding to $v_s = 8002 \pm 22$ m/s, the speed of sound in GaN. Very good agreement between our theoretical modeling and experimental results demonstrates that our theoretical approach, which is a generalization of the Thomsen model,[7] comprehensively describes the dynamics of CAP's in bulk materials, generated by the strong, above-the-bandgap optical excitation and synchronously probed using almost nonattenuated probe pulses. Thus, our above-bandgap pump and far-below-bandgap probe experimental approach makes it possible to successfully generate nanoscale acoustic waves at the surface of bulk semiconductors and, simultaneously, to nondestructively probe the material's structure deeply under its surface. The two-color femtosecond spectroscopy technique, implemented here for the studies of GaN, should be very promising in producing and detecting CAP waves in a large variety of bulk semiconducting materials.

ACKNOWLEDGMENT

The authors would like to thank D. Wang and A. Cross for many valuable discussions throughout the course of this work. S. Wu acknowledges support from the Frank Horton Graduate Fellowship Program. This work was supported by the U.S. Department of Energy Office of Inertial Confinement Fusion under Cooperative Agreement No. DE-FC52-92SF19460, the University of Rochester, and the New York State Energy Research and Development Authority. The support of DOE does not constitute an endorsement by DOE of the views expressed in this article.

REFERENCES

1. Y.-K. Huang *et al.*, Appl. Phys. Lett. **79**, 3361 (2001).
2. R. L. Liu *et al.*, Phys. Rev. B **72**, 195335 (2007).
3. C.-K. Sun, J.-C. Liang, and X-Y. Yu, Phys. Rev. Lett. **84**, 179 (2000).
4. Ü. Özgür, C.-W. Lee, and H. O. Everitt, Phys. Status Solidi B **228**, 85 (2001).
5. G. D. Sanders and C. J. Stanton, Phys. Rev. B **64**, 235316 (2001).
6. O. Matsuda *et al.*, Phys. Rev. B **71**, 115330 (2005).
7. C. Thomsen *et al.*, Phys. Rev. B **34**, 4129 (1986).
8. S. Wu, P. Geiser, J. Jun, J. Karpinski, J.-R. Park, and R. Sobolewski, Appl. Phys. Lett. **88**, 041917 (2006).
9. G. Yu *et al.*, Appl. Phys. Lett. **70**, 3209 (1997).
10. S. Wu, P. Geiser, J. Jun, J. Karpinski, D. Wang, and R. Sobolewski, J. Appl. Phys. **101**, 043701 (2007).
11. C. Deger *et al.*, Appl. Phys. Lett. **72**, 2400 (1998).
12. V. Bougrov *et al.*, in *Properties of Advanced Semiconductor Materials: GaN, AIN, InN, BN, SiC, SiGe*, edited by M. E. Levinshtein, S. L. Rumyantsev, and M. Shur (Wiley, New York, 2001), Chap. 1, pp. 1–30.
13. M. Leszczynski *et al.*, J. Phys. D: Appl. Phys. **28**, A149 (1995).
14. W. Qian, M. Skowronski, and G. S. Rohrer, in *III-Nitride, SiC, and Diamond Materials for Electronic Devices*, edited by D. K. Gaskill, C. D. Brandt, and R. J. Nemanich, Mat. Res. Soc. Symp. Proc. Vol. 423 (Materials Research Society, Pittsburgh, PA, 1996), pp. 475–486.
15. S. L. Chuang and C. S. Chang, Phys. Rev. B **54**, 2491 (1996).
16. G. Tamulaitis *et al.*, Phys. Status Solidi C **3**, 1923 (2006).
17. S. N. Nakamura and G. Fasol, *The Blue Laser Diode: GaN Based Light Emitters and Lasers* (Springer, Berlin, 1997).
18. J. Karpiński, J. Jun, and S. Porowski, J. Cryst. Growth **66**, 1 (1984).